


Self-synchronized temporal-spectral characterization system for revealing ultrafast fiber laser dynamics

YULONG CAO,^{1,2}  ZHENGHU CHANG,¹ QIANG WU,¹ JINGSHENG HUANG,¹ LAIYANG DANG,¹ AI LIU,¹ YIYANG LUO,¹  LIGANG HUANG,¹ WEI HUANG,¹ LEI GAO,^{1,3} AND TAO ZHU^{1,4}

¹Key Laboratory of Optoelectronic Technology & Systems (Ministry of Education), Chongqing University, Chongqing 400044, China

²Department of Electrical and Electronic Engineering, The University of Hong Kong, Hong Kong, China

³e-mail: gaolei@cqu.edu.cn

⁴e-mail: zhutao@cqu.edu.cn

Received 13 October 2022; revised 19 November 2022; accepted 23 November 2022; posted 6 December 2022 (Doc. ID 478095); published 23 January 2023

Due to the electronic bottleneck limited real-time measurement speed of common temporal-spectral detection and the particle-like nature of optical soliton enabled nonrepeatable transient behaviors, capturing the ultrafast laser pulses with unknown times of arrival and synchronously characterizing their temporal-spectral dynamic evolution is still a challenge. Here, using the Raman soliton frequency shift based temporal magnifier and dispersive Fourier transform based spectral analyzer, we demonstrate a self-synchronized, ultrafast temporal-spectral characterization system with a resolution of 160 fs and 0.05 nm, and a recording length above milliseconds. The synchronized nonlinear process makes it possible to image full-filled temporal sub-picosecond pulse trains regardless of their arrival times and without extra pump lasers and photoelectric conversion devices. To demonstrate the significance of this improvement, a buildup dynamic process of a soliton laser with a complex breakup and collisions of multisolitons is visually displayed in the spectral and temporal domains. The soliton dynamic evolution processes observed by our characterization system are in one-to-one correspondence with the numerical simulation results. We believe this work provides a new multidimensional technique to break the electronic bottleneck to gain additional insight into the dynamics of ultrafast lasers and nonlinear science. © 2023

Chinese Laser Press

<https://doi.org/10.1364/PRJ.478095>

1. INTRODUCTION

Ultrafast pulses, localized structures created by the balance between dispersion, nonlinearity, gain, and loss, have served as the cornerstone in spectroscopy [1,2], imaging [3,4], lidar [5], and physical property characterization and manipulation [6,7]. To increase the measurement speed in these applications and provide them with more flexible time, more frequency scales, and operational state intelligently switchable laser sources, new requirements have been put forward for the parameters that control ultrafast pulse lasers and for the dynamic performance of these lasers [8]. However, the particle-like nature of optical solitons enables striking transient behaviors with nonrepeatable phenomena [9,10], which affects the stable operation and performance regulation of a laser. From the insight of frequency domain, thanks to dispersion Fourier transform (DFT) based spectral measurement [11], soliton explosion [12–14], soliton molecules [15–17], and soliton splitting [18,19] have been experimentally studied to comprehend the nonlinear dynamics

that affects the operation of ultrafast lasers. Due to the limited measurement speed of commonly used methods including optical autocorrelation [20], frequency-resolved optical gating (FROG) [21], and spectral phase interferometry for direct electric-field reconstruction (SPIDER) [22], the temporal information of these transient processes has rarely been investigated.

With the development of space-time duality [23], real-time measurement methods in the temporal and spectral domains have provided the foundation and incentive for innovation in many optical metrology fields, from fundamental laser physics to ultrafast precise measurements [24,25]. Parallel to space-time duality based spectral measurement technologies, a temporal ultrafast signal processing system uses a fiber-induced group delay dispersion (GDD) in the time domain to analogize the propagation distance in the spatial domain. Combined with electronic modulators or nonlinear parametric processes [26–29], the quadratic phase modulation has been brought into the time domain as the “lens” to realize the compression,

magnification, or Fourier transform of the temporal envelope [30–33]. Time-lens-based time magnifiers recently have thus begun to play a central role in the fundamental research to deal with the nonlinear propagation of pulses in fibers and microresonators [34,35], which must record long temporal pulse trains with femtosecond resolution. However, the time-lens-based temporal measurement system has always traded off the time NA and resolution [36]. Both asynchronous and synchronous time-lens-based time magnifiers have been developed to resolve the continuous and accurate capture of transient non-repetitive time domain signals under different measurement requirements. For an asynchronous time lens, it is feasible to continuously image the temporal envelope in the time NA on the order of nanoseconds by buffering and replicating the signal being tested and setting a slight difference between the periods of the pump light and the replicated signal light [37]. This approach is suitable for microresonators and has been demonstrated to reveal the dynamics of dissipative Kerr soliton collisions lasting a few nanoseconds [35], but the pulse repetition period of a fiber-based soliton cavity is tens or hundreds of nanoseconds. At this time, the synchronous time-lens-based time magnifiers are more suitable to record thousands of the output round trips of an ultrafast fiber laser. However, most current works are based on opto-electrical detection to obtain the repetition period of the soliton being tested and then use electro-optical modulation (EOM) to regulate the additional pump laser to output pulses with an identical repetition rate, or combine various nonlinear oscillators to generate pump pulses in the same period [26,38]. As a result, the bandwidth of the electronic detection system limits the accuracy of the time synchronization of the pump and the signal to tens of picoseconds, which is mismatched with the pulse duration of the solitons and lacks robustness. In particular, the pulse laser repetition rate is continuously changing during the control of the soliton operation states or soliton interactions

[39,40]. Therefore, exploiting the self-synchronized time magnifier with an all-optical system design with better applicability and compact construction to break the electrical bottleneck is a necessary development trend for ultrafast fiber laser dynamics.

To achieve this goal, we propose and experimentally demonstrate a self-synchronized temporal-spectral characterization (SSTSC) system that combines the Raman soliton frequency shift effect based time magnifier and DFT based time-stretch spectroscopy to overcome the drawback of a single-shot, full-filled detection of a soliton with an unknown time of arrival or rapid evolution. Through this SSTSC system, a 10 millisecond duration of the transient soliton dynamics regardless of the buildup or tuning processes can be characterized from both the time and frequency domains with a resolution of 160 fs and 0.05 nm. At the same time, the nonlinear effect that influences the imaging quality of the parametric time lens (PTL) is also analyzed from the perspective of real-time spectral evolution. As a proof-of-concept demonstration, the buildup dynamic process of an ultrafast laser with complex break-up and collisions of multisolitons is visually displayed by applying our SSTSC system.

2. SYSTEM CONCEPT AND EXPERIMENTAL SETUP

Figure 1 shows how the SSTSC system obtains the self-synchronized pump pulses of PTL and temporal-spectral information of the laser, thereby capturing the soliton dynamics. As a proof-of-concept demonstration, we choose a conventional soliton (CS) as the signal being tested. The spectrum and the pulse trains are shown in Fig. 1. The top path depicts the frequency-to-time mapping through the emerging DFT technique. By inducing the dispersive medium, the spectral envelope of the soliton is continuously reproduced on the timeline at its repetition rate. There is, however, another real-time

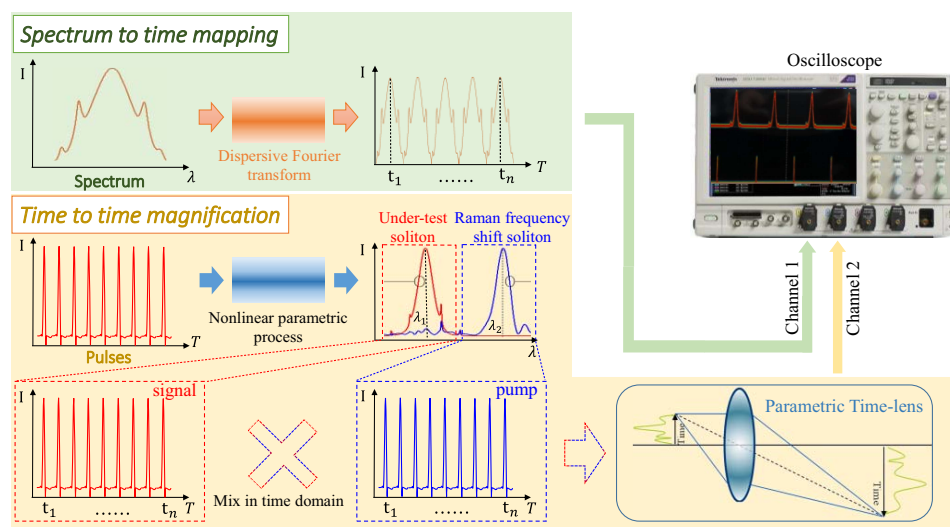


Fig. 1. Schematic representation of the SSTSC system. The single-shot spectrum of every round-trip output pulse will be mapped to the time domain by the DFT (in the green box). The soliton being tested as the input laser source generates the Raman frequency shift soliton with the same repetition rate at a longer wavelength band. The synchronous signal and pump overlap in the time domain and the FWM occurs in PTL to generate the magnification idler pulse to obtain the temporal information of the soliton being tested (in the yellow box).

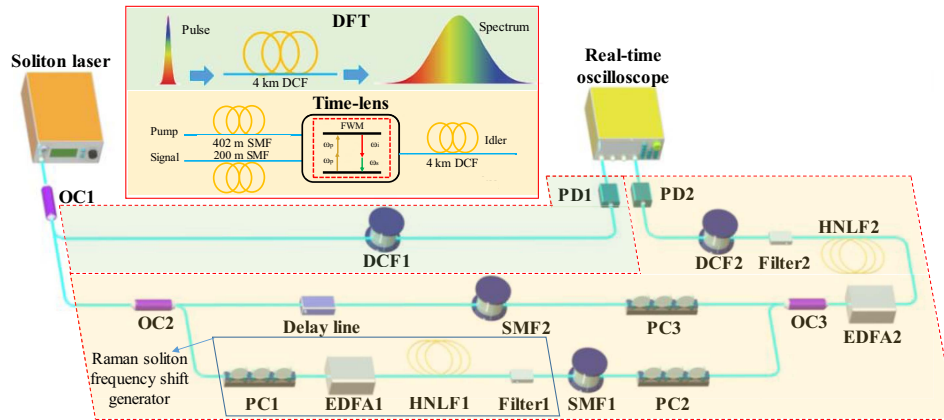


Fig. 2. Schematic diagram of our pulse and spectrum real-time measurement system. The green part is the specific composition and parameter diagram of the DFT system, while the yellow part is the time lens system. The blue solid line box is our Raman soliton frequency shift generator.

spectral measurement method called the parametric spectral-temporal analyzer (PASTA) [41], which uses the spectral-temporal focusing mechanism of a time lens. However, the limitations of the spectral measurement range and four-wave mixing (FWM) conversion efficiency hinder the application of this technology to real-time spectrum measurement of an ultrashort pulse laser with a broad spectral bandwidth. Their complicated clock setting also increases the difficulty of synchronous demodulation with time domain information. As a result, the DFT technique is more convenient for the synchronous detection of an ultrafast fiber laser with MHz repetition rate in our system.

The bottom path displays our Raman soliton frequency-shift-based self-synchronized time lens time magnifier. Using the parametric nonlinear process (soliton self-frequency shift effect) of the Raman-active medium with anomalous dispersion [42–44], the new soliton with the same fundamental repetition rate will be generated at a longer wavelength band. Herein, the principle of this self-synchronized Raman frequency-shift pump soliton generation is as follows. When the ultrashort pulse with high peak power is injected into the high nonlinearity fiber (HNLF), the Raman scattering effect caused by the Stokes light will induce pulse narrowing and obtain the Raman gain from the high-frequency component of soliton spectrum, eventually forming additional fundamental soliton pulse trains. As the pulse propagates, the soliton self-frequency shift occurs with the central wavelength moving toward the longer wavelength side. Because the magnitude of the Raman scattering effect is dependent on the length of the HNLF and the power of the ultrashort pulses, the wavelength of the frequency shift soliton can be tuned by changing these parameters. Namely, we can expediently generate synchronous pump pulses for the soliton pulses being tested with any repetition rate and freely adjust the optical frequency difference between the pump and the signal light to satisfy the phase-matching condition of the nonlinear medium to realize FWM. This “self-synchronization” pulse generated by the soliton itself as the input source through an all-optical process is not limited by the electronic bottleneck, and can accurately locate the soliton to overlap on the timeline

within a several femtosecond time difference [45]. The difference in the dispersion fiber length experienced by the pump, signal and DFT path results in the difference in the round trips between the temporal and spectral information, which can be calculated by the specific fiber length. Figure 2 schematically depicts our real-time measurement system. A detailed description can be found in Visualization 1. Here, the influence of higher-order dispersion effects, especially β_3 , will affect the resolution and system accuracy. In the DFT spectrum measurement path, we can eliminate the error by measuring the dispersion curve of the optical fiber used for dispersion stretching, and then resampling the single-shot spectra [46]. In the PTL path, we can balance the third-order dispersion by configuring fibers with opposite dispersion slopes at the input, output, and pump paths [37].

3. EXPERIMENTAL RESULTS AND DISCUSSION

To demonstrate the performance of the SSTSC system, an ultrafast fiber laser is employed as the soliton being tested. Here, if the idler light is located at a longer wavelength band, when it passes through the dispersion-compensating fiber (DCF) excessive attenuation will be introduced that will reduce the detection sensitivity of the parametric time lens (PTL) system. Therefore, we insert a bandpass filter to restrict the central wavelength of the laser to around 1550 nm. Figure 3(a) shows the autocorrelation trace of the CS mode locked by carbon nanotubes, and the FWHM of the pulse is 1.94 ps. Since the shape of the CS is hyperbolic secant, the real duration of the pulse is ~ 1.26 ps. The spectrum of the CS is shown in Fig. 3(b) with a bandwidth of 2.5 nm and a central wavelength of 1551 nm. The time bandwidth product (TBP) is ~ 0.324 , which is slightly larger than the value of a transform-limited standard of the CS with a sech^2 -shaped pulse (0.315), meaning the soliton is a pulse with a near-zero chirp. The generated Raman soliton frequency shift pulse is filtered by a bandpass optical tunable filter (OTF950, Santec) to act as a pump laser. Because the pump laser is generated by the nonlinear effect of the laser, it will have the same repetition rate as that of the soliton laser. Therefore, compared to a traditional

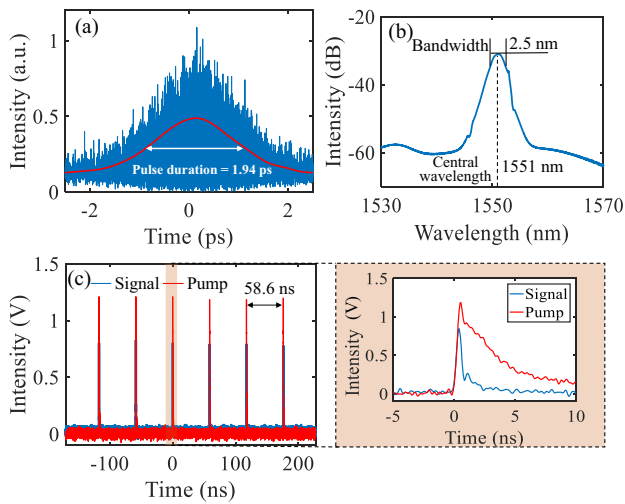


Fig. 3. (a) Autocorrelation trace of the CS being tested. (b) Spectrum of the CS. (c) Pulse trains of the output laser from OC3. The inserted figure is a pair of overlapped signals and pump pulses in Fig. 3(c).

PTL system, our self-synchronized PTL (SS-PTL) system is more convenient to generate the same fundamental frequency pump laser without any electrical equipment like a high-speed photodetector (PD), expensive arbitrary waveform generators, or a broad electronic bandwidth EOM. Figure 3(c) shows that pump pulses and signal pulses completely and perfectly overlap in the time domain. The inserted figure in the dashed box depicts the pair of overlapped signal pulses and the pump pulses in Fig. 3(c). Since the dispersive fiber the pump pulses experience is longer than that for signal pulses, the pulse duration of the stretched pump pulses is broader than that of the signal pulses. This also indicates that the time NA of our PTL system can guarantee that every signal pulse obtains the quadratic phase coefficient carried by the corresponding pump pulse during the subsequent FWM process in the PTL.

The following figures are the key output spectra of the whole process. As can be seen from the red curve in Fig. 4(a), the output of the HNLF1 broadens the spectrum due to the self-phase modulation (SPM), Raman soliton frequency shift, and FWM effect. Then, using a tunable filter with a bandwidth of 4 nm, the main Raman frequency shift soliton is selected as the pump. After the coupling, the overlapped signal and pump have a spectrum with an SNR beyond 30 dB, which is shown by the blue curve in Fig. 4(b). Because the pump and signal pulses are time-stretched by single-mode fibers (SMF1 and SMF2), they can be directly amplified more than 18 dB without any nonlinear spectral degradation, as shown by the red curve in Fig. 4(b). Finally, the cascaded FWM occurs in the HNLF2, which means the quadratic phase delay from the pump has been added to the idler light. The red curve in Fig. 4(c) is the spectrum filtered by Filter2, which carries the temporal information of ~ 304 times magnified signal ($|\varphi_i''/\varphi_s''| \approx 304$). Because the bandwidth of Filter2 is more than 20 nm, the second idler light can also be filtered. The bandwidth of the first idler light is about half of the second one. However, there is almost a 20 dB intensity contrast

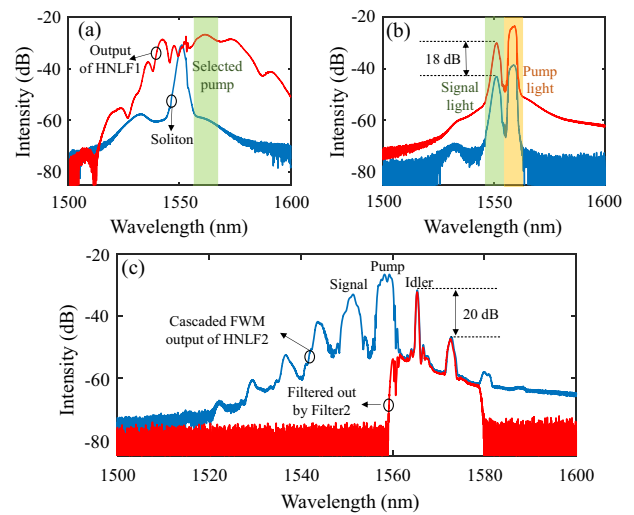


Fig. 4. (a) Average spectrum of the soliton laser and the output of the Raman soliton frequency shift generator. (b) Average spectrum of the overlapping signal and pump (in blue) and the amplified pump and signal (in red). (c) Average spectrum of the FWM and the output from Filter2.

between them. The energy of the second idler light is just 5% of the first idler we wanted. So, the influence of the second idler light can be ignored naturally when using an oscilloscope to acquire the temporal imaging of the soliton pulses.

Then, we perform a temporal-spectral characterization of the CS with a stable mode-locking state. The results are shown in Fig. 5. Both exhibit good temporal-spectral imaging quality and stability. From Figs. 5(a), 5(b) and 5(d), 5(e), the spectrum and pulse evolution of the stable CS are imaged with a frame rate of 17 MHz and temporal magnification of 301. The fluctuations of the integral energy and the bandwidth of single-shot spectrum are about 5%, as depicted in Fig. 5(c). Meanwhile, the fluctuations of the integral energy and temporal duration of every single pulse are about 10%, as depicted in Fig. 5(f). Both the spectral and temporal fluctuations come from the influence of the polarization and power jitter of the erbium-doped fiber amplifier (EDFA).

Among the key parameters of the time magnifier, the temporal imaging frame rate is determined by the repetition period of the soliton laser. Our system has the ability to measure the temporal and spectral information of pulse trains with much higher fundamental frequency. However, when the frame rate increases, the magnification will be limited to avoid the overlapping of the magnified pulses in the time domain. The temporal resolution, which is another key parameter of the SS-PTL system, is determined by the minimum operating electronic bandwidth of the detection system and the designed magnification. In our case, this value is about 160 fs, which is obtained by dividing the minimum detection time of the oscilloscope by the magnification of this time magnifier. Actually, the key parameters of the time-lens based time magnifier can be improved in two ways. First, we can simply increase the operating electronic bandwidth of the detection system to achieve a smaller temporal resolution of the oscilloscope, which of course will greatly increase the system cost.

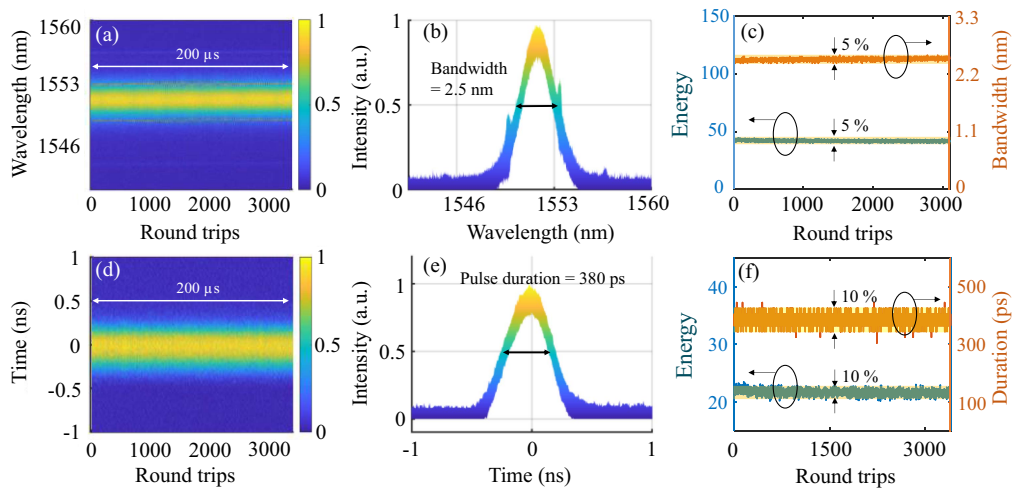


Fig. 5. Spectral evolution of 3100 continuous measurement results of our CS from (a) the top view and (b) the front view. (c) Fluctuations of the spectral energy and bandwidth of 3100 continuous measurement results. Pulse evolution of 3100 continuous measurement results of our CS from (d) the top view and (e) the front view. (f) Fluctuations of the pulse energy and duration of the 3100 continuous measurement results.

What is more, a larger magnification can be designed by increasing (or decreasing) the GDD experienced by idler light (signal light) to improve the system's temporal resolution. This is similar to the space-lens imaging system, which can increase (or decrease) the image distance (object distance) to increase the magnification. In terms of the first method, if the GDD of the signal light is reduced as much as possible, the GDD of the pump light must also be equally reduced at the same time because of the limitation of the imaging formula [26]. However, the time-lens effect is generated by the quadratic phase factor in the time domain introduced by the pump light. When the GDD experienced by the pump light is insufficient to realize the quadratic phase modulation of the idler light during the FWM process, it will cause a temporal imaging distortion. Meanwhile, the GDD experienced by the pump light also determines another key parameter of the time lens: time NA. A small GDD cannot effectively stretch the pump light in the time domain, which reduces the effective overlap time between the pump and the signal during the FWM process, which also limits the range of the final temporal magnification. The second method, which increases the GDD experienced by the idler light, is also subject to two constraints. Similar to the first method, it is also limited by the imaging formula [26]. In addition, excessive GDD will induce a strong fiber insertion loss and reduce the sensitivity of the temporal imaging system. Although the dispersion-to-loss ratio of the fiber can be improved by Raman pump distributed amplification, the nonlinear effects and high-order dispersion accumulated in the long fiber will also distort the temporal imaging pulse trains. Therefore, because of the limitations of these trade-offs, it is difficult to reach a scale below 100 fs for the temporal resolution of time-lens-based time magnifiers, whether synchronous or asynchronous [28,37,38]. To verify that this time magnifier can measure the dynamic evolution of a soliton pulse, we studied the real-time buildup dynamics of the FWM nonlinear process in a PTL system by using the DFT spectroscopy technique, which is described in Visualization 2.

To demonstrate the powerful performance of the self-synchronized temporal-spectral characterization system, the buildup dynamic process of a soliton laser is visually displayed in the spectral and temporal domains with a frame rate of 17 MHz. Figures 6(a) and 6(b) exhibit the spectral information of this unsteady laser evolution process. We only intercept the transition state with the most complex nonlinear phenomenon and the final stable state for analysis. We do not present the preceding *Q*-switched mode-locking state because there is no coherent ultrashort pulse that exists during this state, and we could not detect the time domain information by the SS-PTL system.

From the spectral evolution, we can clearly identify the two well-known nonlinear phenomena accompanied by the establishment of the soliton: the initial spectral broadening caused by the SPM auxiliary pulse mode-locking induced beat dynamics and the wavelength red-shift caused by the Raman effect. Until now, this has been a typical pathway to generate the temporal soliton that has been demonstrated in a Ti:sapphire femtosecond laser cavity and CS cavity based on fiber [11,47]. However, after 1700 round trips, which is shown in Fig. 6(a), the central wavelength of soliton gradually blue shifts and is finally fixed at 1551 nm. This is because we insert a bandpass filter to limit the central wavelength of the laser output to be around 1550 nm. It is worth noting that the wavelength blue shift caused by the filter can prove that the mode-locking laser has the ability to operate at the wavelength sweeping state. When the central wavelength is limited by the inserted filter, the wavelength sweeps continuously, but the mode-locking characteristics in both the time and frequency domains are still maintained in every round trip of the laser output. After soliton stabilization, the spectral bandwidth is about 6 nm. It can be calculated from Fig. 3(b) that the corresponding bandwidth at the 24 dB attenuation of the soliton laser spectrum is also 6 nm. The 24 dB spectral dynamic measurement range is determined by the 8-bit analog-to-digital conversion position of the oscilloscope.

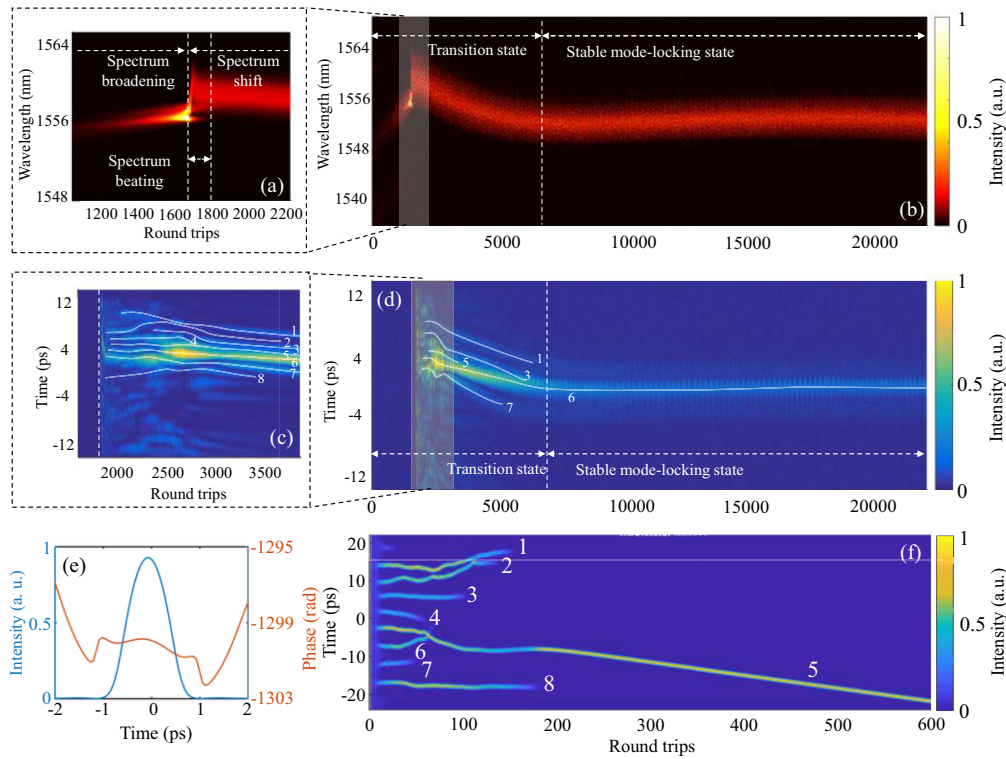


Fig. 6. (a) and (b) Real-time spectrum evolution of a CS buildup process. (c) and (d) Real-time pulse evolution of a CS buildup process. The multipulses are marked by white transparent lines.

Figure 6(a) shows that the red-shifted soliton spectrum occurs at the 1655th round trip, and the spectrum is rapidly broadened to about 6 nm. This indicates that the laser after this round trip gradually formed ultrashort pulses in the time domain, which is demonstrated both in the CS and dissipative soliton (DS) cavities [47,48]. Therefore, the time-lens-based time magnifier starts to work from this time to carry out time domain imaging of ultrashort pulses, obtaining what is shown in Figs. 6(c) and 6(d). From Fig. 6(c), the magnified temporal pulses are generated at the 1810th round trip. The round trip difference is due to the difference in the optical path length of the DFT and SS-PTL systems combined with the fundamental frequency of the laser. Before this stage [before the 1810th round trip in Fig. 6(c)], our time magnifier could not measure any time domain information. This is because, in the absence of coherent soliton pulse generation, the synchronous pump pulses cannot be produced by the Raman self-frequency shift effect for PTL to implement FWM process. During the buildup process of the ultrafast lasers, the time domain information of the relaxation oscillations and spectrum broadening caused by the SPM is composed of nanosecond-interval and picosecond-duration pulses, which can be measured directly by a high-speed photoelectric detection system. However, it is worthwhile to measure the subsequent coherent multipulse generation with a duration less than a picosecond and their fine movement processes using the time magnifier with higher temporal resolution.

Figures 6(c) and 6(d) depict the transient multisoliton states in the time domain during the buildup process of the ultrafast

fiber laser. Eight distinct pulses are generated from the noise known as short-lived soliton molecules. Among them, the No. 6 pulse survives from the competition and eventually evolves into a stable single soliton. During this process, which is depicted in Fig. 6(d), the longer-lived pulses No. 1 and No. 7 preserve the time interval from the main pulse and gradually decay. Meanwhile, the No. 3 and No. 5 pulses gradually approach the main pulse and finally couple with it. We can also observe the collision and annihilation between the pulses from the partially enlarged detail in Fig. 6(c). The noteworthy pulses No. 1 and No. 2 fully demonstrate that the soliton molecules undergo mutual attraction, collision, and final repulsion [49–52], displaying a very complex nonlinear phase evolution in this case. However, the spectral modulation corresponding to soliton molecules does not appear in the real-time evolution spectrum. There may be two explanations for this issue. First, since the integrated energy of the main pulse is one order of magnitude higher than that of other pulses, the modulation depth of the interference spectrum caused by the main pulse and others will be not obvious; and second, the relationship of the free spectrum range (FSR, $\Delta\lambda$) of the interference spectrum of the soliton molecules with the time interval (ΔT) of the pulses is $\Delta T = \lambda_0^2 / (C \cdot \Delta\lambda)$. Here, λ_0 is the central wavelength, and C is the speed of light in vacuum. In our case, the time interval between these adjacent pulses is less than 1 ps. It can be calculated that $\Delta\lambda$ has exceeded 6 nm, which is beyond the spectral bandwidth of the soliton.

To verify the correctness of the experimental results of such soliton buildup dynamics, we established the theoretical model

of the measured CS laser. A detailed description of the simulation model is covered in [Visualization 3](#). Figures 6(e) and 6(f) show the simulation results of the temporal evolution during the CS buildup process. From Fig. 6(f), we find that the multi-soliton pulses during the first 200 round trips are not generated by the soliton splitting, but are directly formed from the noise, which is the same as the experimental results from Figs. 6(c) and 6(d) starting at the 1810th round trip. In this simulation case, the No. 5 pulse survives and eventually evolves into a stable single soliton. Its temporal profile and internal phase are shown in Fig. 6(e), and the pulse duration is about 1.3 ps. The nonlinear phase shift of the stable pulse is smaller than 2 rad, indicating that the No. 5 pulse is a typical CS with little frequency chirp. What is more, we can also observe the No. 1 and No. 2 pulses with mutual attraction, collision, and repulsion behavior in the simulation results, which is similar to the No. 1 and No. 2 pulses in the experimental results. Meanwhile, the No. 6 pulse in Fig. 6(f) gradually approaches the main pulse and finally couples with it. Such pulse evolution behavior is the same as the No. 3 and No. 5 pulses in Figs. 6(c) and 6(d). Finally, the remaining pulses (Nos. 3, 4, 7, and 8) show the same evolutionary behavior as pulses No. 1, No. 7, and No. 8 in the experimental results.

All the simulation results above correspond one-to-one with the multipulse generation and annihilation processes observed in the experiment, thus further verifying the accuracy of our measurement system. By studying soliton buildup dynamics, we have demonstrated the ability of our self-synchronized temporal-spectral characterization system to identify that the emergence of a multipulse state consisting of several distinct soliton-like structures is a typical feature of this soliton buildup process. The experiment and simulation results above highlight the ability of this system to study the multidimensional information measurement of the soliton buildup processes and the self-synchronous detection of nonstationary laser states. In fact, in addition to studying the process mentioned above, the advantages of the system's self-synchronization and multidimensional information acquisition also enable us to explore the laser control dynamics and whether the mode-locked state of the soliton laser can be maintained in real time during continuous parameter regulation. However, limited by the tuning speed of the existing control methods and the storage depth of the oscilloscope, we have not found a suitable experimental scheme to study the limited tuning speed that the mode-locking mechanism can withstand.

4. CONCLUSION

This self-synchronous temporal-spectral characterization system has the powerful function of single-shot full-filled measurement of the spectral and temporal evolution of ultrafast lasers under dynamic change states that last milliseconds. The system takes what we believe, to the best of our knowledge, is an innovative approach, introducing a Raman soliton self-frequency shift effect to generate synchronous pump pulses required by the PTL. This approach greatly reduces the complexity of the time magnifier system and also avoids the necessary conversion of optics to electricity and back to optics in traditional systems. Such an all-optical method provides a fundamental solution to

break the electronic bottleneck limitation and improve the temporal accuracy when solitons are captured with an unknown time of arrival or rapid evolution. As a proof-of-concept demonstration, the buildup process of a CS with transient emergence and decay of coherent multisoliton states is first revealed using experimental and theoretical analyses.

Funding. National Natural Science Foundation of China (61635004, 62075021); National Science Fund for Distinguished Young Scholars (61825501); Chongqing Natural Science Foundation of Innovative Research Groups (CSTC2020JCYJ, CXTTX0005).

Disclosures. The authors declare no conflicts of interest.

Data Availability. Data underlying the results presented in this paper are not publicly available at this time but may be obtained from the authors upon reasonable request.

REFERENCES

1. K. Goda and B. Jalali, "Dispersive Fourier transformation for fast continuous single-shot measurements," *Nat. Photonics* **7**, 102–112 (2013).
2. X. Wei, B. Li, Y. Yu, C. Zhang, K. K. Tsia, and K. K. Y. Wong, "Unveiling multi-scale laser dynamics through time-stretch and time-lens spectroscopies," *Opt. Express* **25**, 29098–29120 (2017).
3. C. Lei, B. Guo, Z. Cheng, and K. Goda, "Optical time-stretch imaging: principles and applications," *Appl. Phys. Rev.* **3**, 011102 (2016).
4. C. Xu and F. Wise, "Recent advances in fibre lasers for nonlinear microscopy," *Nat. Photonics* **7**, 875–882 (2013).
5. Y. Jiang, S. Karpf, and B. Jalali, "Time-stretch LiDAR as a spectrally scanned time-of-flight ranging camera," *Nat. Photonics* **14**, 14–18 (2020).
6. B. Guo, J. Sun, Y. Lu, and L. Jiang, "Ultrafast dynamics observation during femtosecond laser-material interaction," *Int. J. Extreme Manuf.* **1**, 032004 (2019).
7. Y. Jia, S. Wang, and F. Chen, "Femtosecond laser direct writing of flexibly configured waveguide geometries in optical crystals: fabrication and application," *Opto-Electron. Adv.* **3**, 190042 (2020).
8. G. Pu, L. Yi, L. Zhang, C. Luo, Z. Li, and W. Hu, "Intelligent control of mode-locked femtosecond pulses by time-stretch-assisted real-time spectral analysis," *Light Sci. Appl.* **9**, 13 (2020).
9. J. W. Fleischer, M. Segev, N. K. Efremidis, and D. N. Christodoulides, "Observation of two-dimensional discrete solitons in optically induced nonlinear photonic lattices," *Nature* **422**, 147–150 (2003).
10. M. Stratmann, T. Pagel, and F. Mitschke, "Experimental observation of temporal soliton molecules," *Phys. Rev. Lett.* **95**, 143902 (2005).
11. G. Herink, B. Jalali, C. Ropers, and D. R. Solli, "Resolving the build-up of femtosecond mode-locking with single-shot spectroscopy at 90 MHz frame rate," *Nat. Photonics* **10**, 321–326 (2016).
12. A. F. J. Runge, N. G. R. Broderick, and M. Erkintalo, "Observation of soliton explosions in a passively mode-locked fiber laser," *Optica* **2**, 36–39 (2015).
13. H. Chen, M. Liu, J. Yao, S. Hu, J. He, A. Luo, W. Xu, and Z. Luo, "Buildup dynamics of dissipative soliton in an ultrafast fiber laser with net-normal dispersion," *Opt. Express* **26**, 2972–2982 (2018).
14. Y. Cui and X. Liu, "Revelation of the birth and extinction dynamics of solitons in SWNT-mode-locked fiber lasers," *Photon. Res.* **7**, 423–430 (2019).
15. G. Herink, F. Kurtz, B. Jalali, D. R. Solli, and C. Ropers, "Real-time spectral interferometry probes the internal dynamics of femtosecond soliton molecules," *Science* **356**, 50–53 (2017).
16. Z. Wang, K. Nithyanandan, A. Coillet, P. Tchofo-Dinda, and P. Grelu, "Optical soliton molecular complexes in a passively mode-locked fibre laser," *Nat. Commun.* **10**, 830 (2019).

17. Y. Luo, R. Xia, P. Shum, W. Ni, Y. Liu, H. Lam, Q. Sun, X. Tang, and L. Zhao, "Real-time dynamics of soliton triplets in fiber lasers," *Photon. Res.* **8**, 884–891 (2020).
18. X. Liu and M. Pang, "Revealing the buildup dynamics of harmonic mode-locking states in ultrafast lasers," *Laser Photon. Rev.* **13**, 180033 (2019).
19. J. Peng, S. Boscolo, Z. Zhao, and H. Zeng, "Breathing dissipative solitons in mode-locked fiber lasers," *Sci. Adv.* **5**, 1110 (2019).
20. I. Walmsley and C. Dorrer, "Characterization of ultrashort electromagnetic pulses," *Adv. Opt. Photon.* **1**, 308–437 (2009).
21. R. Trebino, K. W. DeLong, D. N. Fittinghoff, J. N. Sweetser, M. A. Krumbügel, B. A. Richman, and D. J. Kane, "Measuring ultrashort laser pulses in the time-frequency domain using frequency-resolved optical gating," *Rev. Sci. Instrum.* **68**, 3277–3295 (1997).
22. C. Iaconis and I. A. Walmsley, "Spectral phase interferometry for direct electric-field reconstruction of ultrashort optical pulses," *Opt. Lett.* **23**, 792–794 (1998).
23. R. Salem, M. A. Foster, and A. L. Gaeta, "Application of space–time duality to ultrahigh-speed optical signal processing," *Adv. Opt. Photon.* **5**, 274–317 (2013).
24. A. Mahjoubfar, D. V. Churkin, S. Barland, N. Broderick, S. K. Turitsyn, and B. Jalali, "Time stretch and its applications," *Nat. Photonics* **11**, 341–351 (2017).
25. B. Li, S. Wang, Y. Wei, S. Huang, and K. K. Y. Wong, "Temporal imaging for ultrafast spectral-temporal optical signal processing and characterization," *IEEE J. Sel. Top. Quantum Electron.* **27**, 7600613 (2021).
26. B. Kolner and M. Nazarathy, "Temporal imaging with a time lens," *Opt. Lett.* **14**, 630–632 (1989).
27. M. Kauffman, A. Godil, and B. Auld, "Applications of time lens optical systems," *Electron. Lett.* **29**, 268–269 (1993).
28. R. Salem, M. Foster, A. Turner, D. F. Geraghty, M. Lipson, and A. L. Gaeta, "Optical time lens based on four-wave mixing on a silicon chip," *Opt. Lett.* **33**, 1047–1049 (2008).
29. T. Ng, F. Parmigiani, M. Ibsen, Z. Zhang, P. Petropoulos, and D. J. Richardson, "Compensation of linear distortions by using XPM with parabolic pulses as a time lens," *IEEE Photon. Technol. Lett.* **20**, 1097–1099 (2008).
30. A. Godil, B. Auld, and D. Bloom, "Picosecond time-lenses," *IEEE J. Quantum Electron.* **30**, 827–837 (1994).
31. J. Howe, J. Hansryd, and C. Xu, "Multiwavelength pulse generator using time-lens compression," *Opt. Lett.* **29**, 1470–1472 (2004).
32. M. Foster, R. Salem, D. Geraghty, A. C. Turner-Foster, M. Lipson, and A. L. Gaeta, "Silicon-chip-based ultrafast optical oscilloscope," *Nature* **456**, 81–84 (2008).
33. B. Li and S. Lou, "Time-frequency conversion, temporal filtering, and temporal imaging using graded-index time lenses," *Opt. Lett.* **37**, 3981–3983 (2012).
34. M. Narhi, B. Wetzell, C. Billet, S. Toenger, T. Sylvestre, J. Merolla, R. Morandotti, F. Dias, G. Genty, and J. Dudley, "Real-time measurements of spontaneous breathers and rogue wave events in optical fibre modulation instability," *Nat. Commun.* **7**, 13675 (2016).
35. Y. Li, S. Huang, B. Li, H. Liu, J. Yang, A. Vinod, K. Wang, M. Yu, D. Kwong, H. Wang, K. Wong, and C. Wong, "Real-time transition dynamics and stability of chip-scale dispersion-managed frequency microcombs," *Light Sci. Appl.* **9**, 1 (2020).
36. B. Kolner, "Space-time duality and the theory of temporal imaging," *IEEE J. Quantum Electron.* **30**, 1951–1963 (1994).
37. B. Li, S. Huang, Y. Li, C. Wong, and K. Wong, "Panoramic-reconstruction temporal imaging for seamless measurements of slowly-evolved femtosecond pulse dynamics," *Nat. Commun.* **8**, 1 (2017).
38. B. Li, J. Kang, S. Wang, Y. Yu, P. Feng, and K. Wong, "Unveiling femtosecond rogue-wave structures in noise-like pulses by a stable and synchronized time magnifier," *Opt. Lett.* **44**, 4351–4354 (2019).
39. F. Kurtz, C. Ropers, and G. Herink, "Resonant excitation and all-optical switching of femtosecond soliton molecules," *Nat. Photonics* **14**, 9–13 (2020).
40. W. He, M. Pang, D. Yeh, J. Huang, C. Menyuk, and P. Russell, "Formation of optical supramolecular structures in a fibre laser by tailoring long-range soliton interactions," *Nat. Commun.* **10**, 5756 (2019).
41. C. Zhang, J. Xu, P. Chui, and K. Wong, "Parametric spectro-temporal analyzer (PASTA) for real-time optical spectrum observation," *Sci. Rep.* **3**, 2064 (2013).
42. D. Skryabin, F. Luan, J. Knight, and P. St.J. Russell, "Soliton self-frequency shift cancellation in photonic crystal fibers," *Science* **301**, 1705–1708 (2003).
43. J. Peng, H. Luo, and L. Zhan, "In-cavity soliton self-frequency shift ultrafast fiber lasers," *Opt. Lett.* **43**, 5913–5916 (2018).
44. N. Nishizawa and T. Goto, "Compact system of wavelength-tunable femtosecond soliton pulse generation using optical fibers," *IEEE Photon. Technol. Lett.* **11**, 325–327 (1999).
45. G. Agrawal, *Nonlinear Fiber Optics, Fourth Edition & Applications of Nonlinear Fiber Optics*, 2nd ed. (Elsevier, 2010).
46. J. Huang, Y. Cao, J. Wang, A. Liu, Q. Wu, Z. Chang, Z. Li, Y. Luo, L. Gao, G. Yin, and T. Zhu, "Time-stretch-based multidimensional line-scan microscopy," *Opt. Laser Eng.* **160**, 107197 (2023).
47. X. Liu and Y. Cui, "Revealing the behavior of soliton buildup in a mode-locked laser," *Adv. Photon.* **1**, 016003 (2019).
48. J. Peng, M. Sorokina, S. Sugavanam, N. Tarasov, D. Churkin, S. Turitsyn, and H. Zeng, "Real-time observation of dissipative soliton formation in nonlinear polarization rotation mode-locked fiber lasers," *Commun. Phys.* **1**, 20 (2018).
49. J. Peng and H. Zeng, "Build-up of dissipative optical soliton molecules via diverse soliton interactions," *Laser Photon. Rev.* **12**, 1800009 (2018).
50. X. Liu, X. Yao, and Y. Cui, "Real-time observation of the buildup of soliton molecules," *Phys. Rev. Lett.* **121**, 023905 (2018).
51. Y. Zhou, Y. Ren, J. Shi, H. Mao, and K. Wong, "Buildup and dissociation dynamics of dissipative optical soliton molecules," *Optica* **7**, 965–972 (2020).
52. P. Ryczkowski, M. Nārhi, C. Billet, J. Meroll, G. Genty, and J. Dudley, "Real-time full-field characterization of transient dissipative soliton dynamics in a mode-locked laser," *Nat. Photonics* **12**, 221–227 (2018).